Received July 2001
Revised November 2001
Accepted November 2001

Influence of non-isothermal fluid properties on the growth of spherical fluid shells

Xundong Qin and Roger E. Khayat
Department of Mechanical and Materials Engineering, Faculty of Engineering Science, The University of Western Ontario, London, Ont., Canada N6A 5B9

Keywords *Fluid, Shells, Lagrangian*

Abstract *This numerical study explores the influence of the time dependence of material fluid parameters on the transient temperature evolution during the growth of fluid shells. The shell is spherical, the fluid is Newtonian, and the flow is induced by a constant driving pressure. The coupled heat and flow equations are solved numerically using the cobody (Lagrangian) transformation and a central difference discretization in space. The range of material values is adjusted from existing experiments. It is generally found that the variation in viscosity, surface tension and specific heat can have a significant influence on both the growth rate and temperature evolution. Thermal conductivity is found to be of little influence.*

Nomenclature

Br	= Brinkman number	$M(T)$	= dimensionless viscosity coefficient
C_0	= reference specific heat, J/(kg K)	N	= number of nodes
C_1, C_2	= constants which are related with k, R_T and R_r	Pe	= Peclet number
$C(T)$	= dimensionless specific heat	q	= radial flux component
C_P	= heat capacity, J/(kg K)	r	= dimensionless radial coordinate
Ca	= capillary number	R	= dimensionless radius of inner surface of the shell
g	= dimensionless surface tension parameter	R_0	= initial radius of the shell, Cm
$G(T)$	= dimensionless surface tension coefficient	$\dot{R}$	= dimensionless velocity of inner surface of the shell
k_0	= reference thermal conductivity, W/(m K)	R_r	= initial outer-to-inner radius ratio
k_T	= thermal conductivity, W/(m K)	R_T	= inner-to-outer surface temperature ratio
k	= dimensionless thermal conductivity parameter	Re	= Reynolds number
$K(T)$	= dimensionless thermal conductivity coefficient	S	= dimensionless radius of outer surface of the shell
m	= dimensionless viscosity parameter	S_0	= initial radius of outer surface, Cm
		$\dot{S}$	= dimensionless velocity of outer surface of the shell

International Journal of Numerical Methods for Heat & Fluid Flow, Vol. 12 No. 2, 2002, pp. 142–162.

DOI 10.1108/09615330210418311

This work is supported by the Natural Sciences and Engineering Research Council of Canada.

t = dimensionless time
t' = transformed dimensionless time
$T(r,t)$ = dimensionless temperature
T_i = dimensionless temperature at inner surface
T_0 = dimensionless temperature at outer surface (reference temperature)
$T_{\max}(t)$ = dimensionless maximum temperature
$u(r,t)$ = dimensionless velocity
V = reference velocity
x = transformed radial coordinate
x_i = ith node position

Greek symbols
Δ = dimensionless ,mesh size
ΔP = typical magnitude of the driving pressure, Pa
μ = viscosity, Kg/(m s)
μ_0 = reference viscosity, Kg/(cm s)
ρ = density, Kg/m^3
ϕ = meridional coordinate
γ = surface tension coefficient, Kg/s^2
γ_0 = reference surface tension coefficient, Kg/s^2
τ^{rr} = dimensionless radial normal stress component
$\tau^{\theta\theta}$ = dimensionless azimuthal normal stress component
$\tau^{\phi\phi}$ = dimensionless meridional normal stress component

Subscripts
r = partial differentiation with respect to radius r
t = partial differentiation with respect to time t

1. Introduction

The numerical simulation of shell growth and collapse remains challenging. This problem is of the moving-boundary type, with the domain moving with time. Research on the growth and collapse of shells and bubbles has a long history. The problem is of considerable fundamental interest in transport phenomena as an example of time-dependent free-boundary problem involving the interaction among heat, mass and momentum transfer. This flow configuration also enjoys several practical applications in industrial processes such as the manufacture of foam and microcellular materials (Strong, 2000), and can be related to blow molding and thermoforming (Ryan and Dutta, 1983).

Microcellular polymers are foam material with cell sizes of less than or equal to 10 μm. They are used in a wide variety of applications such as separation media, adsorbents, controlled release devices and light-weight materials with impact strength (Goel and Thesis, 1993). In forming a microcellular material, a gas such as carbon dioxide (CO_2) is first dissolved into a molten polymer under supercritical conditions, i.e. above the CO_2's critical temperature and pressure, to form a homogeneous polymer solution. Phase separation is then induced by either reducing sharply the pressure or the temperature resulting in the nucleation of a myriad of gas bubbles. The size of the final bubbles depends on several factors such as the number of nucleation sites, the initial gas concentration, the growth dynamics of the bubbles, the polymer properties such as diffusion coefficient, viscosity, elasticity, etc. The theoretical problem of predicting the cell size in foam materials is extremely complex. Some of the specific issues are described below.

One of the fundamental problems is the pressure history in the bubble. Initially, the fluid has to be at high pressure so that nucleation is prevented. Phase separation will start when the pressure falls below a certain threshold. Therefore, the initial pressure in the gas bubble can be taken as the threshold pressure. The difference between the initial fluid pressure and the threshold pressure provides the driving force for the bubble growth. This is the typical approach of earlier researchers. However, this is only the initial driving force. Once the bubble starts to grow, this driving pressure will certainly change, which has to be determined from the diffusion of gas into the bubble. The pressure history in the bubble will then depend on the mass of material accumulated inside, its temperature and the size of the bubble.

Another problem is the effect of viscoelasticity on the growth of the bubble. Even though many researchers agree on some general behavior, the results vary widely with the choice of constitutive equations. One of the difficulties with viscoelasticity is a larger set of equations to be solved and the breakdown of the solution at a finite level of elasticity (Chhabra, 1993). Besides viscoelasticity, the viscosity of the material is also of particular importance, especially the elongational viscosity since the deformation in the bubble is essentially biaxial. The inflation dynamics of a spherical shell is similar to that of the growth or collapse of a spherical gas bubble in an infinite Newtonian or viscoelastic medium; a spherical bubble is just a spherical shell of infinite thickness. Both configurations give rise to biaxial elongational flow. Fogler and Goddard (1970) analyzed the decay of a bubble, initially at rest and later subject to a constant driving pressure for a Maxwell fluid. The elasticity of the fluid surrounding the spherical bubble was found to retard the collapse of the bubble and give rise to a time oscillatory behavior that is absent for a Newtonian fluid. It was also found that the oscillatory motion is particularly enhanced whenever the relaxation time is large compared to the Rayleigh collapse time, i.e. at large Deborah number. Tanasawa and Yang (1970) and Ting (1975) used a three-parameter Oldroyd model (Bird *et al.*, 1987) and predicted a similar behavior. Pearson and Middleman (1977a,b), and later Johnson and Middleman (1978) measured the decay of a bubble, subjected to an initial sudden pressure drop, collapsing in a large polymeric melt. The evolution of the bubble radius was monitored and was found to decay monotonically as in the case of a purely Newtonian fluid. Inertial effects were neglected and no oscillatory behavior was predicted. However, the calculations of Khayat and Garcia-Rejon (1992) for a viscoelastic fluid confirm that, had inertia effects been included in Pearson and Middleman (1977a,b) and Johnson and Middleman (1978), the resulting decay of the bubble radius would have been oscillatory.

Oscillations in statically stressed (that is, under constant driving pressure) viscoelastic fluids, which are absent for Newtonian fluids, are the result of normal stresses (which lead to the Weissenberg rod-climbing phenomenon (Bird *et al.*, 1987)). Recent theoretical and experimental works on polymer melts

and solutions give ample evidence of the existence of oscillatory behavior (Khayat and Garcia-Rejon, 1992). The discrepancy between theory and the experiments of Middleman and coworkers (Pearson and Middleman, 1977a,b; Johnson and Middleman, 1978), particularly the fact that theoretically predicted oscillations are not observed in reality, is fundamentally important. Recently, Khayat (2001) addressed the origin of the discrepancy between theory and experiment for statically stressed systems. In particular, the work focused on the inflation of a spherical shell of a viscoelastic liquid subject to a time-dependent driving pressure.

Other aspects such as compressibility, gas diffusion and non-isothermal influences are also important, but have been largely ignored in the literature (Shafi and Flumerfelt, 1997; Jacobsen and Pierick, 2000). Earlier, Barlow and Langlois (1962) examined the gas diffusion from a Newtonian fluid into an expanding bubble. Street *et al.* (1971) examined the growth of a gas bubble in viscous power-law liquids considering the effect of heat, mass, and momentum transfer. In relation to foam molding, Han and Yoo (1981) modeled the expansion foam by considering the growth of a single bubble in an infinite liquid medium, and conducted experiments as well. Amon and Denson (1984; 1986) introduced a cell model to account for the depletion of gas, with finite amount of liquid being stretched during the bubble expansion in foam processing. More recently, Arefmanesh and Advani (1991) carried out a numerical study based on a polynomial representation of the gas concentration around the bubble under isothermal situations.

Non-isothermal effects have received very little attention despite their impact on bubble and shell dynamics. Arefmanesh and Advani (1995) examined the non-isothermal bubble growth in polymeric foams. There was, however, essentially no discussion of the actual temperature evolution involved. Moreover, the important dissipative mechanism in the energy was neglected. In this study, a systematic numerical examination is attempted to assess the impact of temperature dependence of fluid properties, namely viscosity, surface tension, thermal conductivity and specific heat, on the temperature evolution during the growth of spherical shells of Newtonian fluids. The problem is formulated in Section 2, and the solution procedure is also presented in that section. The influence of the various parameters in the problem is examined in detail in Section 3. Concluding remarks are given in Section 4.

2. Problem formulation and solution procedure

The general equations for a Newtonian fluid spherical shell with the boundary and initial conditions, and the solution procedure are presented in this section. Given the symmetry of the flow, the problem reduces to a transient one-dimensional flow.

2.1 General equations, boundary and initial conditions

The fluid is assumed to be incompressible of density ρ, with viscosity, thermal conductivity, specific heat, and surface tension coefficient that depend on

temperature. The flow is induced by the action of constant driving pressure acting on the inner shell surface. The temperatures at the inner and outer surfaces are assumed to be fixed at T_i and T_0, respectively. The shell is assumed to be confined initially between R_0 and S_0. Let ΔP be the magnitude of the constant driving pressure so that the reference velocity is $V = (\Delta P/\rho)^{1/2}$. The reference length and time are, respectively, the initial radius R_0 of the inner shell surface and R_0/V, while the temperature, T_0, at the outer surface is taken as the reference temperature. The pressure is non-dimensionalized with respect to ρV^2. The temperature dependent specific heat (at constant pressure), C_p, thermal conductivity, k_T, viscosity, μ, and surface tension coefficient, γ, may conveniently be introduced as

$$C_p(T) = C_0 C(T), \quad k_T(T) = k_0 K(T), \quad \mu(T) = \mu_0 M(T), \quad \gamma(T) = \gamma_0 G(T), \tag{1}$$

where C_0, k_0, μ_0 and γ_0 are constants, which will be the reference heat capacity, thermal conductivity, viscosity and surface tension coefficients, respectively. The functions $C(T)$, $K(T)$, $M(T)$ and $G(T)$ will be specified later.

There are five dimensionless groups in the problem, namely the Reynolds number, *Re*, Peclet number, *Pe*, Brinkman number, *Br*, and capillary number, *Ca*. These are explicitly and, respectively, given by

$$Re = \frac{\rho V R_0}{\mu_0}, \quad Pe = \frac{R_0 V \rho C_0}{k_0}, \quad Br = \frac{\mu_0 V^2}{k_0 T_0}, \quad Ca = \frac{\mu_0 V}{\gamma_0}. \tag{2}$$

There are two remaining quantities as well, the initial outer-to-inner surface radius ratio, R_r, and the inner-to-outer surface temperature ratio, R_T, which are, respectively, given by

$$R_r = \frac{S_0 - R_0}{R_0}, \quad R_T = \frac{T_i}{T_0}. \tag{3}$$

Additional dimensional parameters will be introduced when the materials properties are further discussed. The relevant equations (and flow variables) for the problem are the conservation of mass, radial momentum, and energy equations, which are written in dimensionless form

$$u_r + 2\frac{u}{r} = 0, \tag{4}$$

$$Re(u_t + uu_r) = -Re\, p_r + \tau_r^{rr} + \frac{1}{r}(2\tau^{rr} - \tau^{\theta\theta} - \tau^{\phi\phi}), \tag{5}$$

$$Pe\, C(T)(T_t + uT_r) = -q_r - 2\frac{q}{r} + Br\left[\tau^{rr} u_r + (\tau^{\theta\theta} + \tau^{\phi\phi})\frac{u}{r}\right], \tag{6}$$

where the following dimensionless variables are introduced, namely, r, the radial position, t, the time, $u(r,t)$, the radial velocity component, $p(r,t)$, the pressure, $T(r,t)$, the temperature, $\tau^{rr}(r,t)$, $\tau^{\theta\theta}(r,t)$, $\tau^{\phi\phi}(r,t)$, the normal stress

components, and the radial flux component, q. A subscript denotes partial differentiation. For a Newtonian fluid, the normal stress components are given (in dimensionless form) by

$$\tau^{rr} = 2M(T)u_r, \quad \tau^{\theta\theta} = \tau^{\phi\phi} = 2M(T)\frac{u}{r}. \tag{7}$$

The fluid is assumed to obey Fourier's law, so that

$$q = -K(T)T_r. \tag{8}$$

At any time t, the fluid occupies the region of a spherical shell of inner and outer radii $R(t)$ and $S(t)$, respectively. The boundary conditions for the problem are prescribed as follows. The kinematic conditions at the inner and outer surfaces are, respectively,

$$u(r = R, t) = \dot{R}, \quad u(r = S, t) = \dot{S}, \qquad \forall t > 0, \tag{9}$$

where a dot denotes total differentiation. Since the temperature is prescribed, then

$$T(r = R, t) = R_T, \quad T(r = S, t) = 1, \qquad \forall t > 0. \tag{10}$$

In this case, the dynamic conditions may be written as

$$-Re\, p(R, t) + \tau_{rr}(R, t) - \frac{2G(R_T)}{Ca\, R(t)} = -Re, \quad \forall t > 0, \tag{11a}$$

$$-Re\, p(S, t) + \tau_{rr}(S, t) - \frac{2G(1)}{Ca\, S(t)} = 0, \quad \forall t > 0, \tag{11b}$$

In the present work, the air inside the shell is assumed to be motionless. Conditions (11a) and (11b) are derived under equilibrium conditions. Their validity under dynamic conditions is usually simply assumed. For further discussion on the validity of this assumption, the reader is referred to Batchelor (1961) and Park and Homsy (1984).

Finally, regarding the initial conditions, the fluid is assumed to be initially at rest, so that

$$u(r, t \leq 0) = 0, \quad \forall r \in [1, R_r]. \tag{12}$$

The temperature is assumed to obey the steady-state distribution, which satisfies condition (10). In other words,

$$T(r, t \leq 0) = \frac{(-1 + \sqrt{1 - 2k(C_1/r + C_2)})}{k}, \quad \forall r \in [1, R_r], \tag{13}$$

where $C_1 = R_T[(k/2)(R_T + 1) + 1]$ and $C_2 = -((k/2) + 1) - R_T[(k/2)(R_T + 1) + 1]$ are constant, k being a material constant (see below). The problem is now reduced to an initial-value system.

2.2 Reduced equations

Integration of equation (4) and use of condition (9) lead to the following expressions:

$$u(r,t) = \frac{\dot{R}(t)R^2(t)}{r^2} = \frac{\dot{S}(t)S^2(t)}{r^2}, \quad \forall r \in [R(t), S(t)]. \tag{14}$$

Integration of equation (5) over the interval r, $r \in [R(t), S(t)]$, eliminating the radial traction from conditions (11a) and (11b), and the radial velocity component from equation (14), give

$$Re\left[R(R\ddot{R} + 2\dot{R}^2)\left(\frac{1}{R} - \frac{1}{S}\right) - \frac{1}{2}(R^2\dot{R})^2\left(\frac{1}{R^4} - \frac{1}{S^4}\right)\right]$$

$$= Re + 4F(1)\frac{\dot{R}}{R}\left(\frac{R^3}{S} - 1\right) - \frac{2}{Ca}\left(\frac{G(1)}{S} + \frac{G(R_T)}{R}\right)$$

$$+ 4\dot{R}R^2\int_R^S \left(\frac{M'T_r}{r^3}\right)\mathrm{d}r, \tag{15}$$

where a prime denotes total differentiation with respect to the temperature. It is observed, from equation (14), that the evolution of the outer surface radius is related to $R(t)$ through

$$S(t) = [R(t)^3 - 1 + (R_r + 1)^3]^{1/3}. \tag{16}$$

The energy equation (6) is accordingly reduced to:

$$Pe\,C\left(T_t + \frac{\dot{R}R^2}{r^2}T_r\right) = K'T_r^2 + K\left(\frac{2}{r}T_r + T_{rr}\right) + 12Br\,M\left(\frac{\dot{R}R^2}{r^3}\right)^2. \tag{17}$$

Equations (15)–(17) constitute a coupled nonlinear algebraic–intro-differential system, where $R(t)$, $S(t)$ and $T(r,t)$ must be solved simultaneously. The initial-value problem is now achieved by using a finite-difference discretization in r for the temperature.

2.3 Solution procedure

It is convenient to introduce first the Lagrangian coordinates (x, t') according to

$$r = (x + R^3)^{1/3}, \quad t = t', \tag{18}$$

which is a transformation that is originally due to Epstein and Plesset (1950). This transformation is useful as it allows the spatial integration to be carried out over a fixed interval $x \in \lfloor 0, (R_r + 1)^3 - 1\rfloor$ as opposed to the time-dependent interval $r \in [R(t), S(t)]$. Furthermore, the transformation allows the elimination of the convective term in the energy equation (17), leading to

$$Pe\,CT_t = 9K'(x+R^3)^{4/3}T_x^2 + 12Br\,M\frac{\dot{R}^2R^4}{(x+R^3)^2} + K\left[12(x+R^3)^{1/3}T_x + 9(x+R^3)^{4/3}T_{xx}\right]. \quad (19)$$

Equation (19) is reduced to a set of ODEs by using an implicit central difference discretization along x. Thus,

$$Pe\,C_i\frac{\mathrm{d}T_i}{\mathrm{d}t} = 9K_i'(x_i+R^3)^{4/3}\left(\frac{T_{i+1}-T_{i-1}}{\Delta}\right)^2 + 12Br\,M_i\frac{R^4\dot{R}^2}{(x_i+R^3)^2} + K_i\left(12(x_i+R^3)^{1/3}\frac{T_{i+1}-T_{i-1}}{\Delta} + 9(x_i+R^3)^{4/3}\frac{T_{i+1}-2T_i+T_{i-1}}{\Delta^2}\right), \quad (20)$$

where T_i is the temperature at the ith node positioned at x_i, $C_i = C(T_i)$, $K_i = K(T_i)$ and $M_i = M(T_i)$. Here $\Delta = x_{i+1} - x_{i-1}$ is the mesh size. It turned out that a fixed increment, $\Delta = 2[(R_r+1)^3 - 1]/N$, was entirely sufficient to obtain numerical stability in the solution procedure, where N is the number of nodes.

Upon substitution for S from equation (16), and discretization of the integral in equation (15), the system of equations (15) and (20) constitutes an initial-value problem with N degrees of freedom, with initial conditions as follows. The initial radii of the inner and outer surfaces of the shell are fixed such that

$$R(t=0) = 1. \quad (21)$$

Since the fluid is initially at rest, then

$$\dot{R}(t=0) = 0. \quad (22)$$

The initial values for T_i follow from equation (13) and transformation (18), to give

$$T_i(t=0) = \frac{-1 + \sqrt{1 - 2k\left(\dfrac{C_1}{\left(\dfrac{i\Delta}{2}+R^3\right)^{1/3}} + C_2\right)}}{k}, \quad i \in [1,N]. \quad (23)$$

The integral in equation (15) is discretized using Simpson's rule. A sixth-order Runge–Kutta scheme (IMSL–DIVPRK) is applied to integrate the resulting set of ODEs from equations (15) and (20). The accuracy of the solution was checked using Gear's predictor–corrector method (IMSL–DIVPAG). The results from

both methods are essentially identical when the same time increment is used. In both methods, a tolerance of less than 10^{-6} is used. That is, the norm of the local error is controlled such that the global error is less than the tolerance imposed. Additional accuracy assessment is reported below.

3. Numerical results

In this section, the evolution of the flow field and the simultaneous heat convection are determined for a spherical shell subject to a constant driving pressure. The shell is supposed to be initially in equilibrium under the action of an internal pressure and surface tension. The influences of the temperature dependence of fluid properties on the shell growth will be examined in some detail. The overall flow and temperature fields are first discussed, allowing the general assessment of the accuracy and convergence of the numerical implementation. In all results reported here, the value of the initial aspect ratio is fixed at $R_r = 1$, which corresponds to a relatively thick shell. The level of pressure is reflected in the value of Re. The outer surface is assumed to remain at a colder temperature, $T(S,t) = 1$, while the inner surface is assumed to be twice as hot, so that $R_T = 2$ and $T(R,t) = 2$. This configuration is encountered in typical cavity growth problems, such as during foam molding and extrusion. The temperature-dependent material functions in equation (1) are assumed to be of the form (Arefmanesh and Advani, 1995; Deen, 1998)

$$C(t) = 1 + cT, \tag{24}$$

$$G(T) = 1 - gT, \tag{25}$$

$$K(T) = 1 + kT, \tag{26}$$

$$M(T) = \exp(m/(T - 0.5)), \tag{27}$$

where c, g, k and m are constants that reflect the strength of the temperature dependence.

3.1 Overall behavior and numerical assessment

Consider the response in thermal and flow behavior for an inflating shell with moderately large inertia ($Re = 10$), and relatively negligible surface tension ($Ca = 10$). In this case, $Br = Pe = 100$. The material parameters are set at $c = 0.4$, $k = 0.1$, $m = 1$ and $g = 50$. Figure 1 displays the evolution of the inner and outer radii $R(t)$ and $S(t)$, as well as that of the thickness, $h(t) = S(t) - R(t)$, with time. The shell growth is typically of the exponential type, and therefore emphasis will be on the early transients. It is interesting to observe that $h(t)$ tends to decrease essentially linearly with time. The rate of growth is reflected in Figure 2 through $\dot{R}(t)$ and $\dot{S}(t)$. It is clear, and as expected, that $\dot{R}(t) > \dot{S}(t)$. In general, the inner surface moves 30% faster than the outer surface, leading to the thinning and eventual breakup of the shell. It is

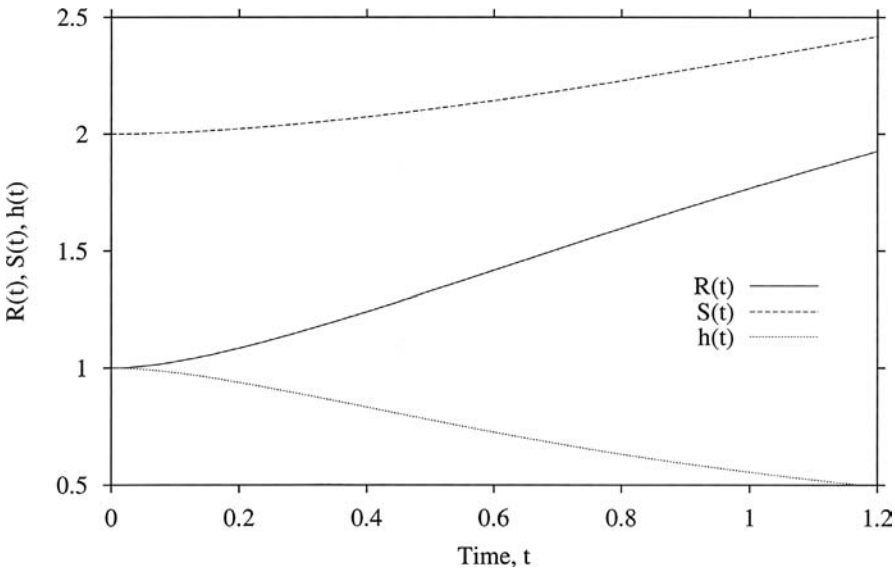

Figure 1.
Evolution of the inner and outer radii, $R(t)$ and $S(t)$, as well as the thickness, $h(t)$, with time for $Br = Pe = 100$, $Ca = Re = 10$ and $R_r = 1$ ($c = 0.4$, $k = 0.1$, $m = 1$ and $g = 50$)

interesting to observe that the outer surface tends to accelerate monotonically with time, while the inner surface experiences a relatively strong acceleration initially. The velocity of the inner surface, however, increases initially with time, reaching a maximum, and decreases thereafter. In the long term, the two surfaces accelerate essentially at the same rate.

The evolution of the temperature distribution is shown in Figure 3, where $T(r, t)$ is plotted against r at different time stages. The temperature tends to exhibit a maximum at any time stage. There is a sharp increase near the inner surface, indicating strong dissipation near $r = R(t)$. The maximum becomes increasingly localized with time because of the thinning of the shell. However, the temperature gradient remains consistently higher near the inner surface. This is resulting from the presence of strong dissipation, which in turn is due to the relative dominance of $\dot{R}(t)$. The evolution of the temperature is further understood from Figure 4, where $T(x, t)$ is plotted against t at different radial locations between $x = 0$ and $x = 7$ (recall that the interval for x does not change with time). The figure shows that the temperature (excluding the boundary points) increases generally with time, reaches a maximum and begins to decrease. The rate of increase appears to be essentially the same at any location initially. The intricate behavior near $r = R(t)$ or $x = 0$ is the result of the interplay among convection, diffusion and dissipation. In order to understand the behavior near the inner surface, first note from equation (7) and Figure 3 the locations $x = 0.2$ and 0.4 are essentially upstream of where the maximum in temperature occurs. In this region, the temperature gradient is very steep and positive, thus making the convective effect dominant.

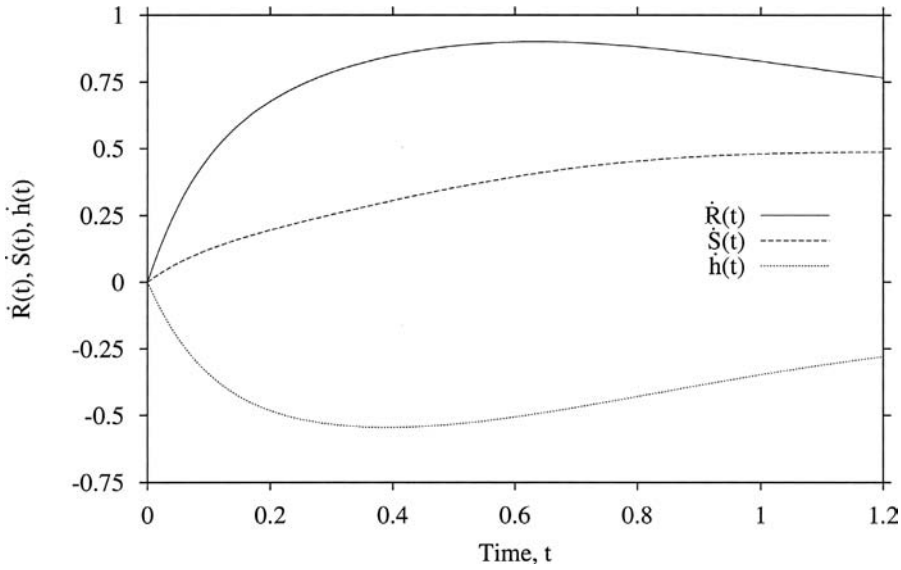

Figure 2.
Evolution of the rate of growth of inner and outer surfaces, and the thickness of the spherical shell, for the same parameter values as in Figure 1

Dissipation is also significant since the velocity is large and the radius is relatively small. Thus the convective and dissipative terms in equation (7) tend to be in balance with each other, leaving the growth in T essentially proportional to the diffusive term. However, Figure 3 clearly indicates that the concavity is small near $r = R(t)$ so that the $\partial T/\partial t$ remains eventually constant since it behaves like $T(r = R, t)$. At the location of the maximum in

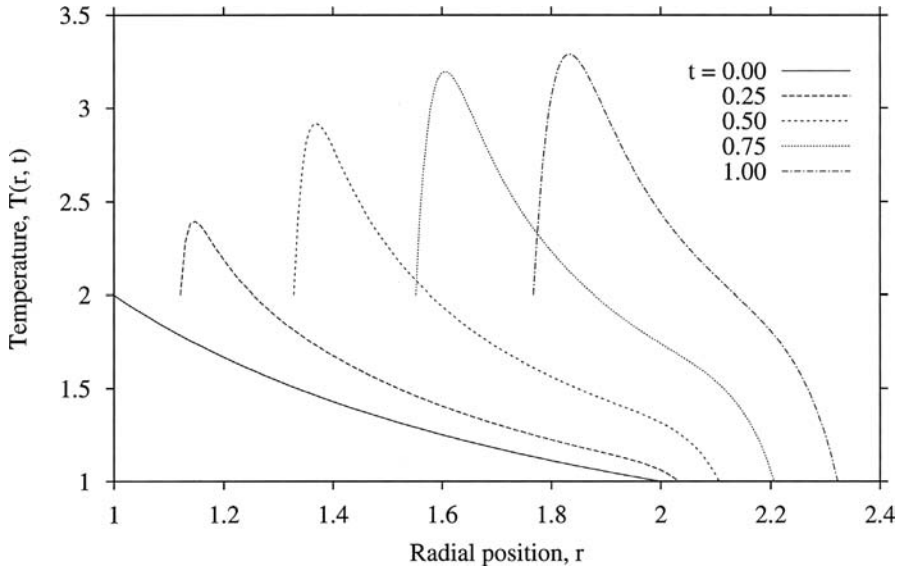

Figure 3.
Temperature distribution across the shell at different time stages, for the same parameter values as in Figure 1

temperature, the rate of growth of T is dictated by the dissipative term (small curvature), which for the present case ($Pe = Br = 100$) dominates entirely the diffusive term. For a point located further downstream, that is after the maximum in temperature is reached, the convective term becomes increasingly important (as r increases), but this time its effect adds to dissipation, leading to the significant growth rate in T that is depicted in Figure 4.

The accuracy of the method is mainly influenced by the spatial discretization of the energy equation, and the approximation used to evaluate the integral in the momentum equation. The integration with time is handled practically to any desired level of accuracy. It is generally found that the influence of the mesh size in the radial direction is rather insignificant. Convergence is essentially achieved by using 100 nodes for $x \in [0, 7]$. Figure 5 shows the influence of N on the temperature distribution, as well as the positions of the inner and outer surfaces, at $t = 0.75$ as in Figure 3. It is observed that even with $N = 20$, the overall temperature distribution is captured except perhaps near the maximum; for $r > 1.65$. For $N = 80$, the temperature estimated at the mesh nodes is fairly accurate; however, more resolution is needed. The distributions based on $N = 100$ and 140 are essentially identical.

3.2 Influence of viscosity

The dependence of the viscosity on temperature is expected to have a significant effect on both the flow and temperature behaviors. It is helpful to first assess the dependence strength of the viscosity on T. This is shown in

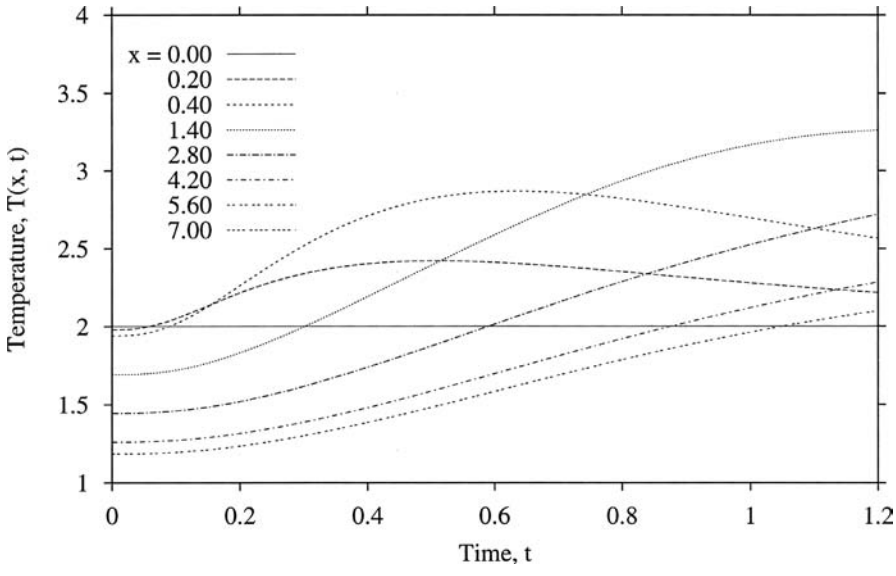

Figure 4.
Evolution of the temperature for different radial locations between $x = 0$ and $x = 7$, for the same parameters as in Figure 1

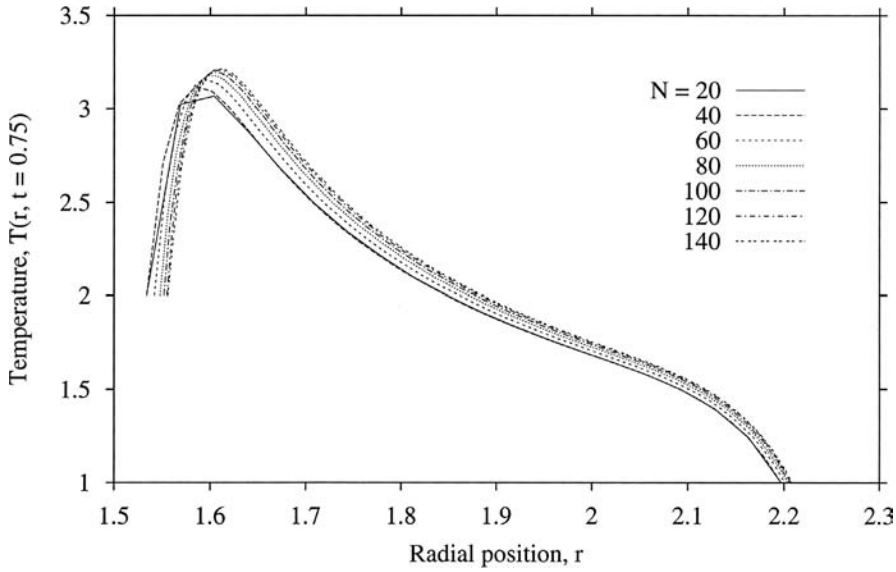

Figure 5.
Influence of mesh size on the temperature distribution at $t = 1.25$ for the same parameter values as in Figure 1

Figure 6, where the viscosity coefficient, $M(T)$, is plotted against T between 1 and 3.5 and $m \in [-2, 2]$. It is observed that the viscosity remains essentially constant for $T > 2$. There is a sharp decrease in M for T near 1. Although the rate of decrease is not strongly influenced by m, the viscosity drops more sharply for $m = 2$. The influence of viscosity on the shell growth is depicted in Figure 7 for $Br = Pe = 100$, $Ca = Re = 10$ and $R_r = 1$ ($c = 0.4$, $k = 0.1$, and $g = 5$), where R and h are plotted against t. The figure shows a dramatic change in growth behavior as m changes sign. For negative m, the growth is of exponential type, similarly to the response for fluids with constant viscosity ($m = 0$). The shell grows (and the thickness decreases) generally faster as m decreases. However, there is little change in R or h for $m < -1$. For positive m, the shell grows (and h drops) linearly with time at a rate that diminishes significantly with m. It is thus interesting to observe that the growth and thinning of the shell can be inhibited by temperature dependence of viscosity. The corresponding temperature distributions are shown in Figure 8 at $t = 1$. Here the effect of m is even more significant. For instance for $m = -2$ and -1, the shell evolution is essentially the same (see Figure 7), but the temperature distribution shows a significant difference (more than 20%). Generally, as m increases, the viscosity increases and the temperature buildup lessens, eventually leading to no shell growth, with the temperature remaining essentially unchanged ($m = 2$). There is, however, a non-monotonic effect of m that becomes evident by inspecting $T_{\max}$. Figure 9 displays the evolution of $T_{\max}(t)$, which shows that the maximum increases with m for $m < 0$, and decreases for $m > 0$. In fact, for $m = 2$, there is no maximum (see also

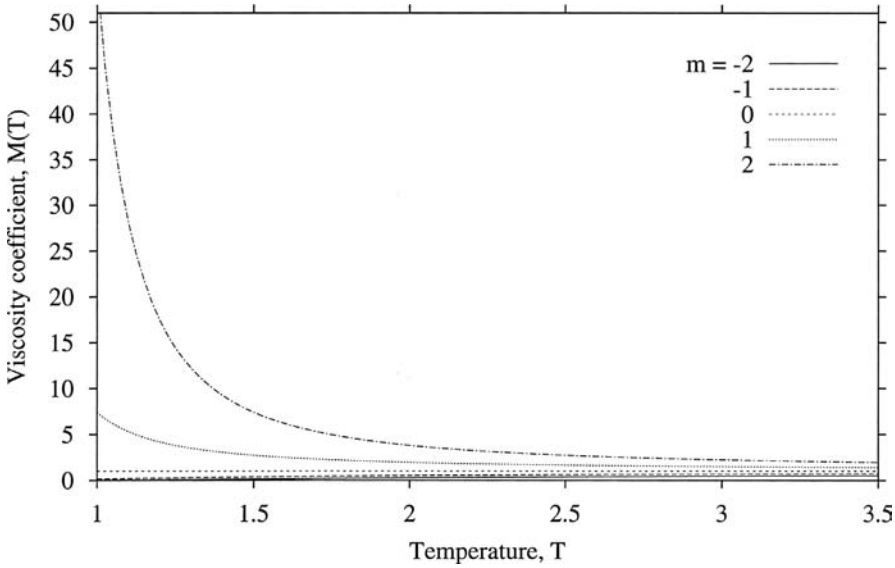

Figure 6.
Dependence of viscosity coefficient, $M(T)$, on temperature for $m \in [-2, 2]$

Figure 8). The non-monotonicity is clearly illustrated in Figure 10, where $T_{\max}$ is plotted against m at different time stages. Note that at $t = 0$, $T(t) = 2$.

3.3 Influence of surface tension

The influence of the surface tension coefficient, g, on the shell growth and thickness is depicted in Figure 11 for $Br = Pe = 100$, $Ca = Re = 10$ and $R_r = 1$

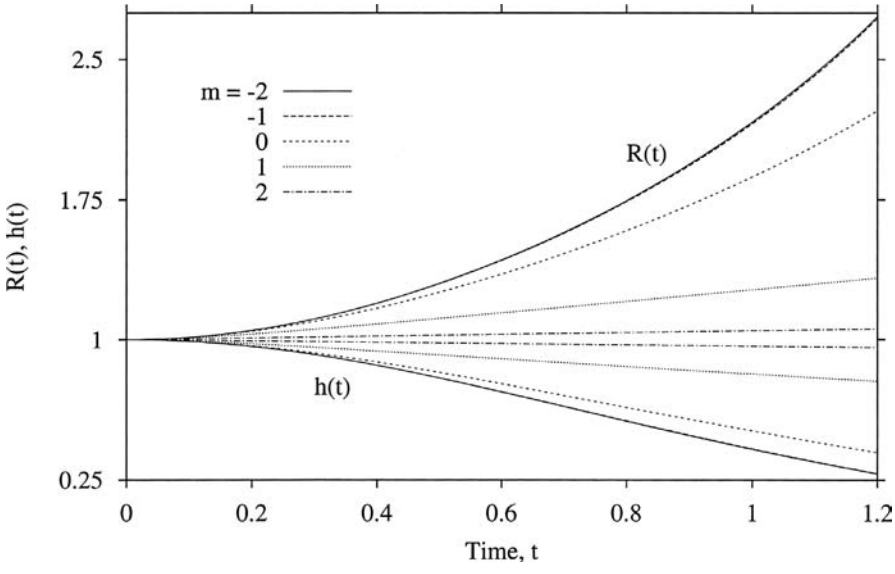

Figure 7.
Influence of viscosity on the evolution of the inner radius, $R(t)$, and thickness, $h(t)$, for $m \in [-2, 2]$, $Br = Pe = 100$, $Ca = Re = 10$ and $R_r = 1$ ($c = 0.4$, $k = 0.1$, and $g = 5$). Note that the upper and lower set of curves correspond to R and h, respectively

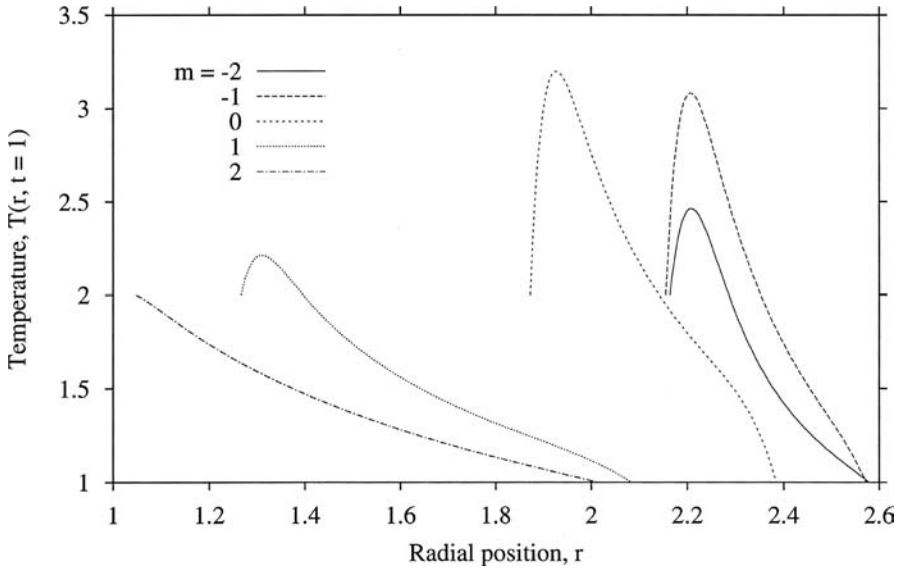

Figure 8.
Influence of viscosity on the temperature distribution at $t = 1$ for the same parameters as in Figure 7

($c = 0.4, k = 0.1$, and $m = 1$). It is recalled from equation (25) that surface tension effect decreases as g increases. Thus, as expected, the shell tends to grow and thin faster with g. However, the effect of g seems to be essentially linear on both R and h. There is a similar strong influence of g on the temperature distribution across the shell. Figure 12 shows the behavior $T(r, t = 1)$ against r for every g. The temperature increases with g as a result from additional

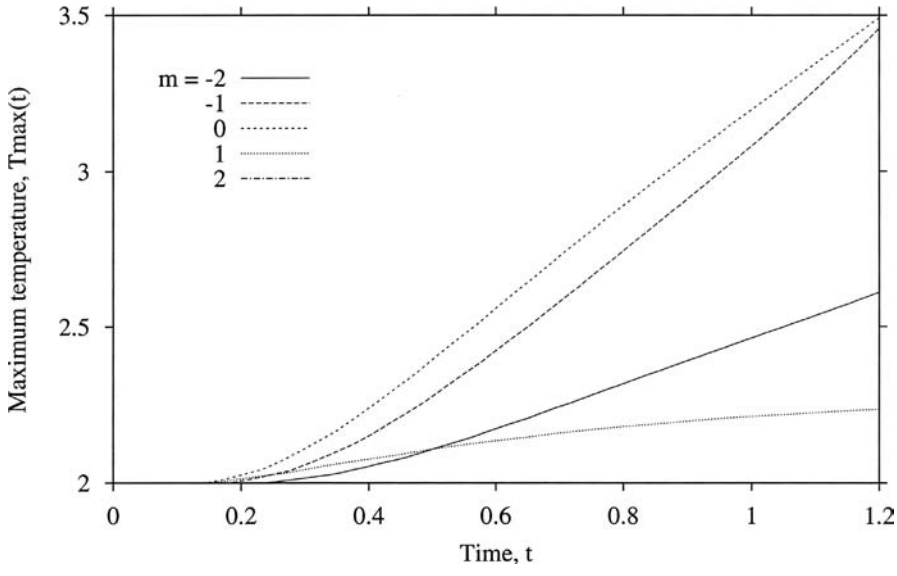

Figure 9.
Influence of viscosity on the evolution of the temperature maximum for the same parameters as in Figure 7

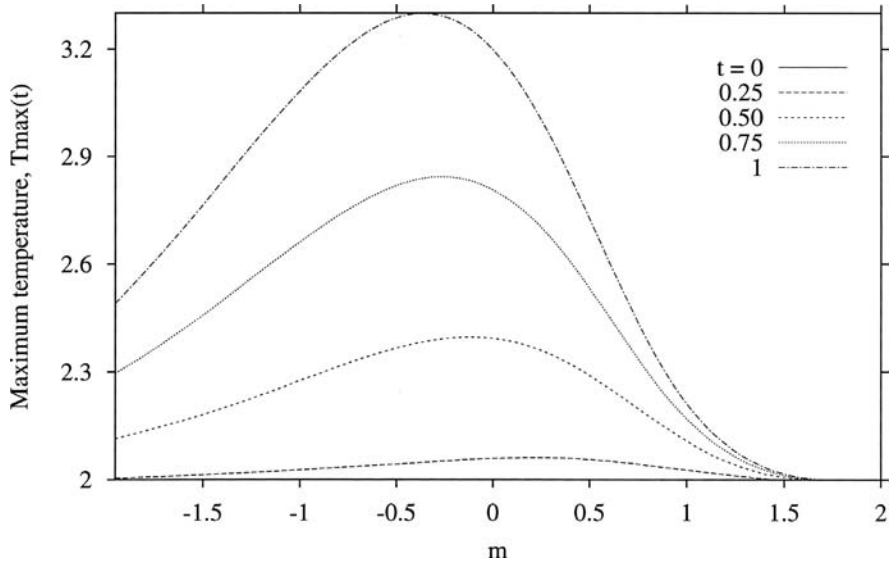

Figure 10.
Dependence of the temperature maximum on m, at different time stages, for the same parameters as in Figure 7

dissipation. The influence of g is again linear as confirmed from Figure 13, which shows the dependence of $T_{\max}(t)$ on g for different time stages.

3.4 Influence of thermal conductivity

It is generally found that the thermal conductivity has little influence on the flow and shell growth. Calculations are carried out for $Br = Pe = 100$,

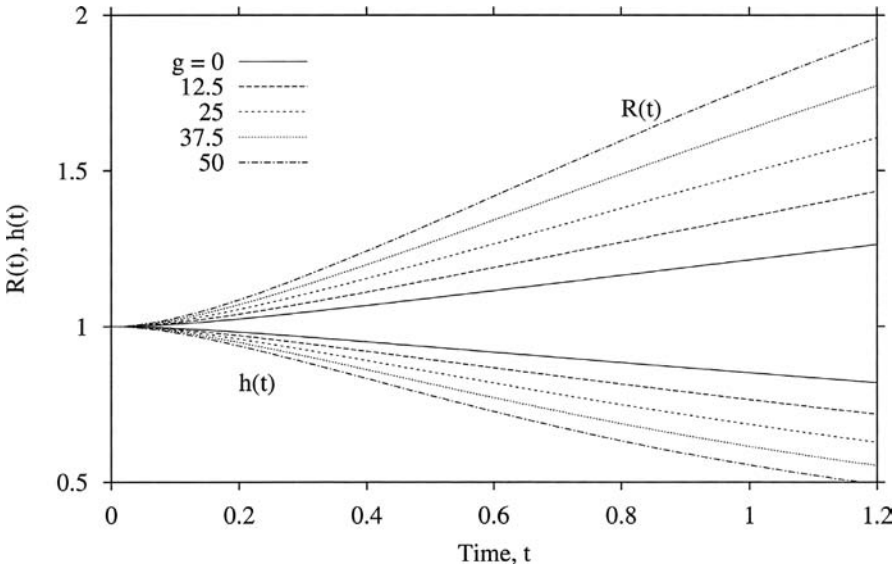

Figure 11.
Influence of surface tension on the evolution of the inner radius, $R(t)$, and thickness, $h(t)$, for $g \in [0, 50]$, $Br = Pe = 100$, $Ca = Re = 10$ and $R_r = 1$ ($c = 0.4$, $k = 0.1$, and $m = 1$). Note that the upper and lower set of curves correspond to R and h, respectively

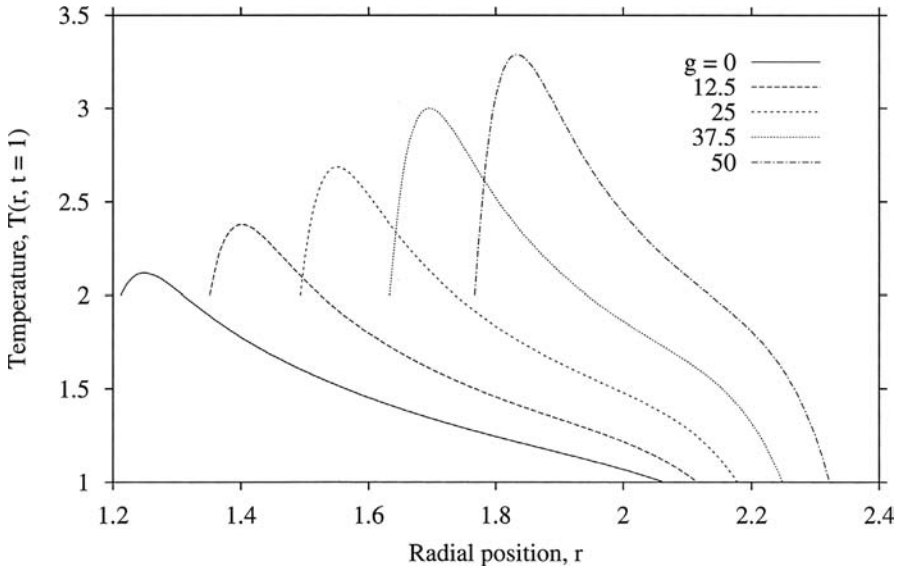

Figure 12.
Influence of surface tension on the temperature distribution at $t = 1$ for the same parameters as in Figure 11

$Ca = Re = 10$ and $R_r = 1$ ($c = 0.4$, $g = 50$, and $m = 1$). Figure 14 displays the influence of k on the temperature distributions at different time stages. A high k value tends to lower linearly the temperature buildup, but not as significantly as g, at least for the range of materials considered here. It is interesting to observe from the figure that the influence of k becomes more significant under

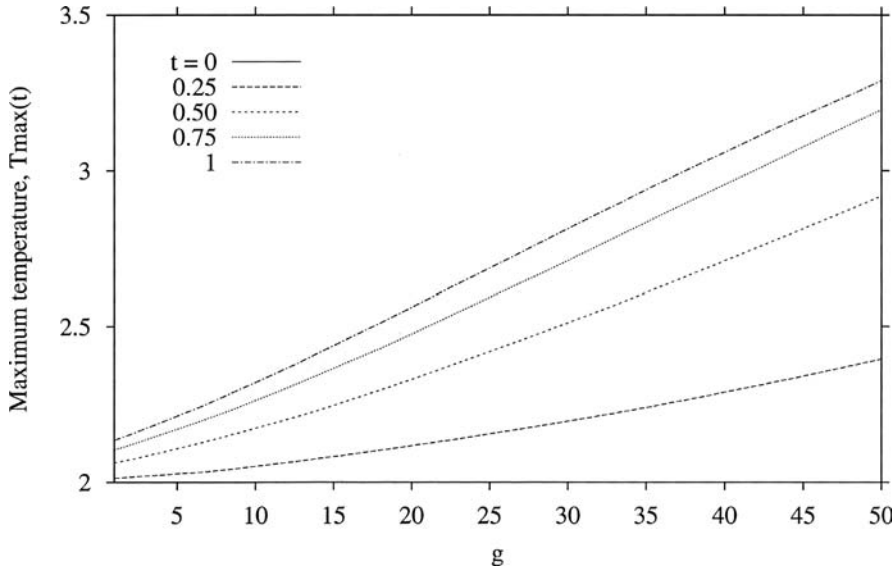

Figure 13.
Dependence of the temperature maximum on g, at different time stages, for the same parameters as in Figure 11

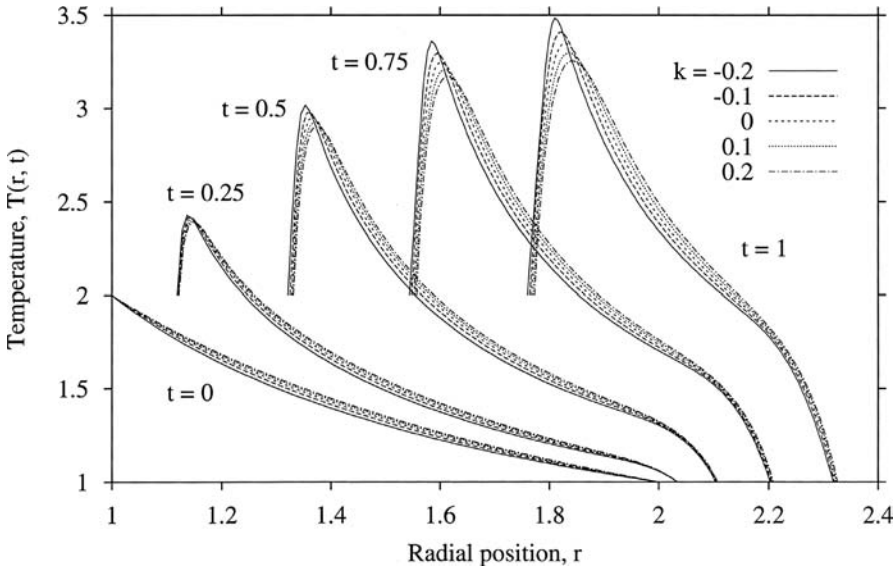

Figure 14.
Influence of thermal conductivity on the temperature distribution at different time stages for $k \in [-0.2, 0.2]$, $Br = Pe = 100$, $Ca = Re = 10$ and $R_r = 1$ ($c = 0.4$, $g = 50$, and $m = 1$)

transient conditions. Figure 15 depicts the linear decrease in $T_{\max}(t)$ with k at different time stages. Note the sharper drop with k as t increases.

3.5 Influence of the specific heat

The influence of specific heat is reflected in Figures 16–18 for $Br = Pe = 100$, $Ca = Re = 10$ and $R_r = 1$ ($g = 50$, $k = 0.1$, and $m = 1$). A fluid with higher

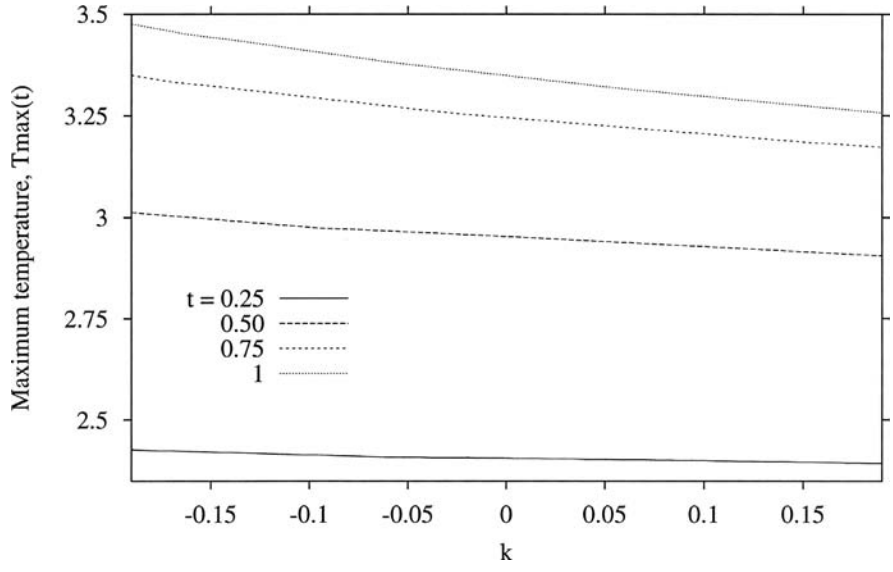

Figure 15.
Dependence of the temperature maximum on k, at different time stages, for the same parameters as in Figure 14

specific heat tends to grow slower, as depicted from Figure 16. However, the influence of the coefficient c decreases significantly for $c > 1$. This is also confirmed from Figure 17, where the temperature distributions are plotted for different time stages. While the growth is slightly diminished by increasing c, the temperature buildup is significantly decreased, particularly at the later time stages, as also inferred from Figure 18.

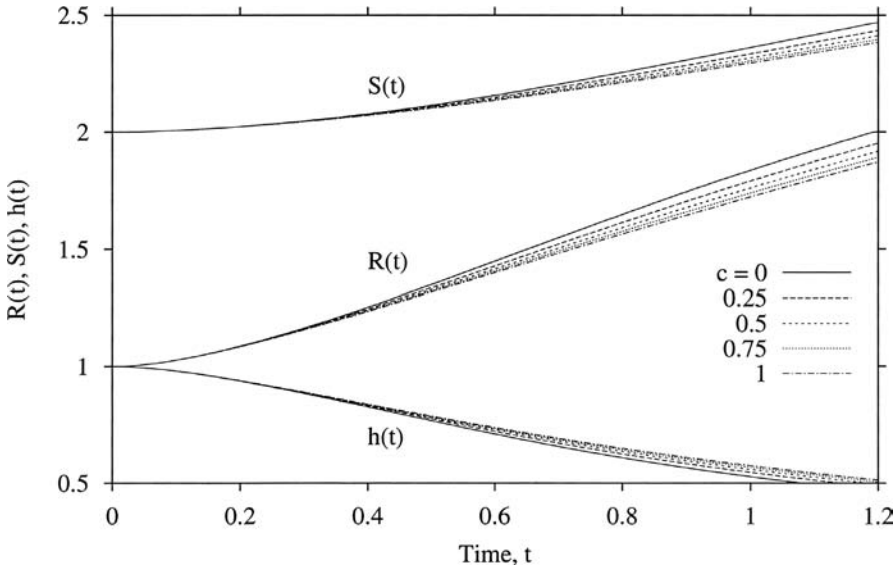

Figure 16.
Influence of specific heat on the evolution of $R(t)$, $S(t)$ and $h(t)$ for $c \in [0, 1]$, $Br = Pe = 100$, $Ca = Re = 10$ and $R_r = 1$ ($g = 50$, $k = 0.1$, and $m = 1$)

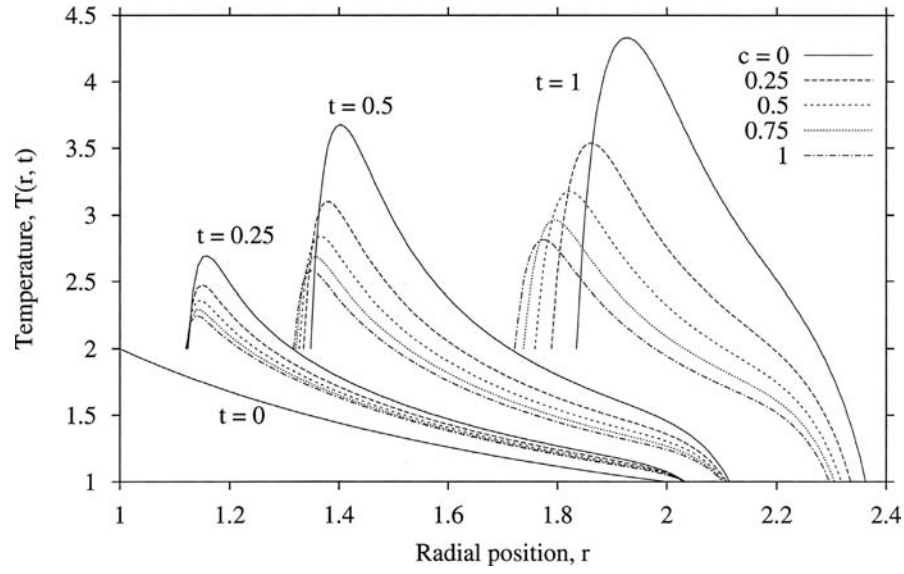

Figure 17.
Influence of specific heat on the temperature distribution at different time stages for the same parameters as in Figure 16

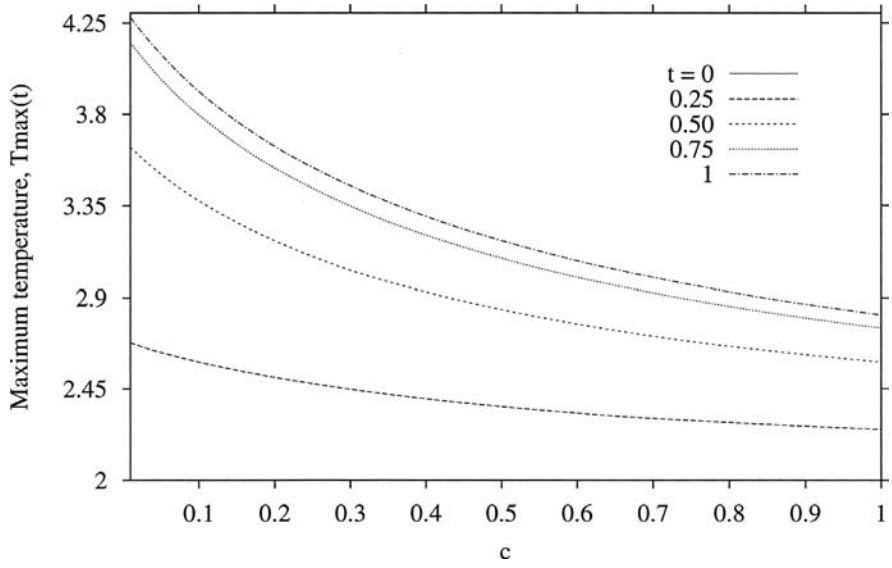

Figure 18.
Dependence of the temperature maximum on *c*, at different time stages, for the same parameters as in Figure 16

4. Conclusion

The present study focuses on the transient temperature and flow fields during the growth of spherical shells of Newtonian fluids, under the action of constant driving pressure. The flow and heat transfer are coupled through the temperature dependence of the fluid properties. This thermo-mechanical coupling is expected to emerge in processing such as foaming and blow molding. The influence of viscosity, surface tension, thermal conductivity and specific heat is particularly emphasized, with close examination of the temperature buildup during flow.

References

Amon, M. and Denson, C.D. (1984), *Polym. Eng. Sci.*, Vol. 24, p. 1026.

Amon, M. and Denson, C.D. (1986), *Polym. Eng. Sci.*, Vol. 26, p. 255.

Arefmanesh, A. and Advani, S.G. (1991), "Diffusion-induced growth of a gas bubble in a viscoelastic fluid", *Rheol. Acta*, Vol. 30, p. 274.

Arefmanesh, A. and Advani, S.G. (1995), "Nonisothermal bubble growth in polymeric foams", *Polym. Eng. Sci.*, Vol. 35, p. 252.

Barlow, E.J. and Langlois, W.E. (1962), *IBM J.*, Vol. 6, p. 329.

Batchelor, G.K. (1961), *Introduction to Fluid Dynamics*, Cambridge University Press, Cambridge.

Bird, R. B., Armstrong, R.C. and Hassager, O. (1987), *Dynamics of Polymeric Liquids*, 2nd ed., Wiley, New York Vol. 1.

Chhabra, R. P. (1993), *Bubble, Drops, and Particles in Non-Newtonian Fluids*, CRC Press, Boca Raton, FL.

Deen, W.M. (1998), *Analysis of Transport Phenomena*, Oxford University Press, Oxford.

Epstein, P.S. and Plesset, M.S. (1950), "On the stability of gas bubbles in liquid-gas solutions", *J. Chem. Phys.*, Vol. 18, p. 1505.

Fogler, H.S. and Goddard, J.D. (1970), "Collapse of spherical cavities in viscoelastic fluids", *Phys. Fluids*, Vol. 13, p. 135.

Goel, S.K., Ph.D. thesis, University of Pittsburgh, Pittsburgh, PA.

Han, C.D. and Yoo, H.J. (1981), *Polym. Eng. Sci.*, Vol. 21, p. 518.

Jacobsen, K. and Pierick., D. (2000), Microcellular foam molding: advantages and application examples, *SPE Annual Technical Conference, present volume*.

Johnson, E.D. and Middleman, S. (1978), *Polym. Eng. Sci.*, Vol. 18, p. 963.

Khayat, R.E. (2001), "Oscillatory behavior in statically stressed viscoelastic inflation flow", *Quart. J. Mech. Appl. Math.*, Vol. 54, p. 599.

Khayat, R.E. and Garcia-Rejon, A. (1992), "Uni- and bi-axial unsteady inflation of a viscoelastic material", *J. Non-Newtonian Fluid Mech.*, Vol. 43, p. 31.

Park, W.C. and Homsy, G. (1984), "Two-phase displacement in Hele-Shaw cells; theory", *J. Fluid Mech.*, Vol. 139, p. 291.

Pearson, G.H. and Middleman, S. (1977a), *AIChE J.*, Vol. 23, p. 714.

Pearson, G.H. and Middleman, S. (1977b), *AIChE J.*, Vol. 23, p. 722.

Ryan, M.E. and Dutta, A. (1983), *Polym. Eng. Sci.*, Vol. 22, p. 569.

Shafi, A. and Flumerfelt, R.W. (1997), "Initial bubble growth in polymer foam process", *Chem. Eng. Sci.*, Vol. 52, p. 627.

Street, J.R., Fricke, A.L. and Reiss, L.P. (1971), *Ind. Eng. Chem. Fund.*, Vol. 10, p. 54.

Strong, A. B. (2000), *Plastics: Materials and Processing*, 2nd ed., Prentice Hall, Upple Saddle River, NJ, p. 0.

Tanasawa, I. and Yang, W.J. (1970), "Dynamic behavior of a gas bubble in viscoelsatic liquids", *J. Appl. Phys.*, Vol. 41, p. 4526.

Ting, R.Y. (1975), "Viscoelastic effect of polymers on single bubble dynamics", *AIChE J.*, Vol. 21, p. 810.